Journal of Sound and Vibration (2003) **259**(1), 193–208
doi:10.1006/jsvi.2002.5154, available online at http://www.idealibrary.com on IDEAL®

LETTERS TO THE EDITOR

EFFECTS OF NUMERICAL DISSIPATION AND DISPERSION ON ACOUSTIC PREDICTIONS FROM A TIME-DOMAIN FINITE DIFFERENCE TECHNIQUE FOR NON-LINEAR WAVE DYNAMICS

N. S. Dickey and A. Selamet

Department of Mechanical Engineering, The Ohio State University, 206 West 18th Ave., 43210-1107, Columbus, OH 43210-1107, *U.S.A. E-mail*: *selamet.1@osu.edu*

AND

K. V. Tallio

Powertrain Operations, Ford Motor Company, Dearborn, MI 48126, *U.S.A.*

(*Received* 28 *January* 2002, *and in final form* 25 *February* 2002)

1. INTRODUCTION

Non-linear one-dimensional approaches are useful for modelling the unsteady flows in the breathing systems of internal combustion engines. These computational techniques have been extensively used in the automotive industry to predict the influence of intake and exhaust system geometry on engine performance parameters such as power output and volumetric efficiency [1–5]. As expected, the non-linear techniques can also be used to predict the acoustic characteristics and radiated sound for the intake and exhaust systems. The non-linear computations can include several phenomena that are not adequately treated by more traditional linear acoustic approaches such as valve flows, mean values and their gradients, convective non-linearities, wave steepening and flow losses. These factors, and particularly the highly non-linear flows through the valves and in the primary manifold runners, are important for predicting radiated sound levels.

A variety of commercial, proprietary and research codes for modelling one-dimensional flow in the duct systems of automotive engines are currently in use. It is generally recognized that when used appropriately, these methods are capable of predicting cycle-averaged engine performance parameters with good accuracy [1–5]. When used to predict radiated sound levels, however, these techniques have been somewhat less successful. At lower frequencies (below roughly 500 Hz), radiated sound levels are often predicted well while at higher frequencies the results are generally viewed as unreliable.

A fundamental reason that these techniques do not perform well at high frequencies is the assumption of one-dimensional fluid motion. This assumption fails when the wavelength λ is comparable to the transverse dimensions of an intake or exhaust system element. Since $\lambda = c/f$, where c is the speed of sound and f is the frequency, the one-dimensional assumption limits the frequency range for which the analysis applies. In addition, localized multi-dimensional motions may be important at sudden changes in cross-sectional area, and in complicated geometric structures. Provided that non-linear effects in the regions with multi-dimensional motions are small, non-linear and linear

0022-460X/02/$35.00

techniques can be coupled to overcome limitations from the one-dimensional assumption [6, 7]. Including multi-dimensional effects in this manner is attractive since the non-linear (and primarily one-dimensional) flows at the valves and primary runners can be included, while a non-linear three-dimensional simulation of the entire system, which is impractical for predictive tools, is avoided.

Another important, yet less discussed cause of inaccuracies in radiated sound predictions is the behavior of the numerical schemes themselves. Specifically, the numerical errors are due to the combined effects of: (1) the characteristics of the numerical schemes and (2) how the schemes are applied in practice (the spatial and temporal discretization). The selection of a numerical approach and how to apply it is a compromise between the competing needs of accuracy, stability, speed and computational requirements. For simulations of small acoustic disturbances, high order schemes may be applied to achieve good accuracy and efficiency with a relatively coarse mesh. Higher order schemes are more computationally complex, however, and can experience stability problems for the non-linear physics and rapidly changing boundary conditions in intake and exhaust system simulations. Thus, the majority of numerical methods applied for intake and exhaust system simulations have been simpler, but less accurate (for a given mesh) first or second order techniques. In addition, the accuracy of a simulation is typically judged with respect to predictions of cycle-averaged performance parameters such as volumetric efficiency, torque and power. Then, to minimize computational time, the grid is typically set at the coarsest value that will give the required accuracy in engine performance predictions. Such a grid, however, is likely to be insufficient for higher frequency acoustic disturbances.

The objective of this study is to investigate the performance of a representative finite-difference approach for small-amplitude disturbances. The investigation focuses on the computational phase and amplitude errors incurred for sinusoidal disturbances propagating in a stationary and inviscid medium. The explicit finite-difference technique of Chapman and co-workers [5, 8] is applied for the non-linear balance equations of mass, momentum and energy. This finite difference approach has been used extensively in design tools for automotive intake and exhaust systems [5, 9]. Moreover, the basic behavior of this approach is expected to be representative of a number of finite-difference schemes that have been applied to duct flows in internal combustion engines (Lax-Wendroff, MacCormack, etc.) [10–13].

2. BACKGROUND

In a finite-difference technique for compressible flows, the differential balance equations for mass, momentum and energy, coupled with an equation of state, are approximated over discrete intervals in time and space. In most cases, the finite-difference approximations will approach the original equations as the timestep (Δt) and node spacing (Δx) approach zero. Since the timestep and nodal spacing must be finite, there will always be some discrepancy between the original equations and finite-difference solution. The overall discrepancies for a system of non-linear equations (as in the present study) are difficult to determine analytically, and are beyond the scope of this work (see, for example, references [14, 15]). However, the fundamental concepts can be demonstrated from the analysis of a simpler linear equation.

A simplified model for wave propagation is given by the linear convection equation

$$\frac{\partial p}{\partial t} + c_0 \frac{\partial p}{\partial x} = 0, \tag{1}$$

where t is the time, x is the axial co-ordinate and, from an acoustic viewpoint, p is the acoustic (perturbation) pressure and $c_0 \geqslant 0$ is the mean speed of sound, which is a constant. Equation (1) thus represents the ideal translation of a simple acoustic wave in the positive x direction at velocity c_0. For a single-frequency harmonic disturbance entering the left boundary and passing freely through the right boundary, an exact solution is given by

$$p(x,t) = P_0 e^{-ik_0 x} e^{i\omega t}, \tag{2}$$

where P_0 is an amplitude constant, i is the imaginary unit, $k_0 = \omega/c_0$ is the wavenumber, $\omega = 2\pi f$ is the angular frequency and f is the frequency.

A first order accurate finite-difference representation for equation (1) is given by (see Appendix A)

$$\frac{p_j^{n+1} - p_j^n}{\Delta t} + c_0 \frac{p_j^n - p_{j-1}^n}{\Delta x} = 0, \tag{3}$$

where the subscript j denotes a spatial index and superscript n denotes a temporal index. Inspection of the two finite-difference terms in equation (3) indicates that the approximate expression approaches the original differential equation as Δt and Δx approach zero. However, direct inspection tells little about the differences between the discrete and continuous equations, or the effects of the relative sizes of Δt and Δx. Additional information is available from the modified equation, which represents the differential equation that is actually being solved by the finite-difference representation. The modified equation can be obtained by inserting Taylor series expansions for p_j^{n+1} and p_{j-1}^n into equation (3) which, after rearrangement, gives

$$\frac{\partial p}{\partial t} + c_0 \frac{\partial p}{\partial x} + \left[\frac{\partial^2 p}{\partial t^2}\left(\frac{\Delta t}{2!}\right) + \frac{\partial^3 p}{\partial t^3}\left(\frac{\Delta t}{3!}\right)^2 + \cdots \right] + c_0 \left[-\frac{\partial^2 p}{\partial x^2}\left(\frac{\Delta x}{2!}\right) + \frac{\partial^3 p}{\partial x^3}\left(\frac{\Delta x}{3!}\right)^2 - \cdots \right] = 0. \tag{4}$$

A comparison of equations (4) and (1) clearly shows that the leading terms of the truncation error for the finite-difference expression are of order Δt and Δx. To more easily compare the behavior of the modified equation to the solution given by equation (2), the spatial derivative terms in equation (4) are systematically eliminated using higher derivatives of the modified equation as[†]

$$[\text{equation (4)}] + \left(\frac{\Delta x}{2}\right)\frac{\partial}{\partial x}[\text{equation (4)}] - \left(\frac{\Delta x}{2c_0}\right)\frac{\partial}{\partial t}[\text{equation (4)}] + \left(\frac{(\Delta x)^2}{12}\right)\frac{\partial^2}{\partial x^2}[\text{equation (4)}] - \left(\frac{(\Delta x)^2}{3c_0}\right)\frac{\partial^2}{\partial x \partial t}[\text{equation (4)}] + \left(\frac{(\Delta x)^2}{3c_0^2} - \frac{\Delta x \Delta t}{4c_0}\right)\frac{\partial^2}{\partial t^2}[\text{equation (4)}]. \tag{5}$$

With the introduction of the Courant number,

$$\mathscr{C} = \frac{c_0 \Delta t}{\Delta x}, \tag{6}$$

[†] For an initial value problem with periodic boundary conditions, the temporal derivatives are eliminated [14, 16].

equation (5) can be arranged as

$$\frac{\partial p}{\partial t} + c_0 \frac{\partial p}{\partial x} + (\mathscr{C} - 1)\frac{\Delta x}{2c_0}\frac{\partial^2 p}{\partial t^2} + (\mathscr{C}^2 - 3\mathscr{C} + 2)\left(\frac{(\Delta x)^2}{6c_0^2}\right)\frac{\partial^3 p}{\partial t^3} + O[(\Delta t)^3, (\Delta t)^2 \Delta x, \Delta t(\Delta x)^2, (\Delta x)^3] = 0. \tag{7}$$

Note that when $\mathscr{C} = 1$, the first- and second order truncation error terms in equation (7) are zero. For this equation, the higher order truncation error terms are also zero for $\mathscr{C} = 1$, and the modified equation is identical to the original differential equation.

If terms of higher order than $(\Delta t)^2$ and $(\Delta x)^2$ are ignored, a solution to equation (7) consistent with the exact solution given by equation (2) is

$$\tilde{p}(x,t) = P_0 \mathrm{e}^{-\mathrm{i}k_0(1-\mathrm{i}\omega(\Delta x/2c_0)(1-\mathscr{C})-\omega^2((\Delta x)^2/6c_0^2)(\mathscr{C}^2-3\mathscr{C}+2))x}\mathrm{e}^{\mathrm{i}\omega t}, \tag{8}$$

where the superscript $\sim$ has been used to denote the approximate solution. For the boundary conditions considered, the discretization errors can be interpreted in terms of a modified wavenumber k as

$$k = k_0\left(1 - \mathrm{i}\omega\frac{\Delta x}{2c_0}(1-\mathscr{C}) - \omega^2\frac{(\Delta x)^2}{6c_0^2}(\mathscr{C}^2 - 3\mathscr{C} + 2)\right). \tag{9}$$

The deviation of k from k_0 has both imaginary and real components. The imaginary component is the result of odd derivatives in the truncation error and leads to amplitude errors while the real component is due to the even derivative terms and result in phase errors, or numerical dispersion. As indicated by equation (8), $k = k_0$ when $\mathscr{C} = 1$.

Taking the ratio of equations (8) and (2) and introducing the wavelength $\lambda = 2\pi c_0/\omega$ gives

$$\frac{\tilde{p}(x,t)}{p(x,t)} = \underbrace{\mathrm{e}^{-\pi(\Delta x/\lambda)(1-\mathscr{C})k_0 x}}_{\text{Amplitude error}} \quad \underbrace{\mathrm{e}^{\mathrm{i}(2\pi^2/3)(\Delta x/\lambda)^2(\mathscr{C}^2-3\mathscr{C}+2)k_0 x}}_{\text{Phase error}}, \tag{10}$$

where the separate terms contributing to amplitude and phase errors have been denoted. Equation (10) illustrates several characteristics of the approximate solution that are commonly seen in explicit finite difference schemes used in internal combustion engine simulations. As might be expected, errors due to spatial discretization are frequency dependent, and are sensitive to the ratio between Δx and λ. Thus, for a fixed nodal spacing, errors will increase as the frequency increases and the number of nodes per wavelength decreases. Equation (10) also indicates that errors for any value of $\Delta x/\lambda$ will be zero when $\mathscr{C} = 1$. While this finding does not directly apply to the more complex system of equations being solved in internal combustion engine simulations, numerical accuracy will typically improve as $\mathscr{C}$ approaches an upper limit for the numerical approach. However, $\mathscr{C}$ needs to remain below this limit to ensure numerical stability. The primary dependence of numerical stability on $\mathscr{C}$ for the simple first order scheme is evident in the amplitude error term of equation (10). For $\mathscr{C} > 1$, the finite-difference approximation gives an unbounded exponentially increasing function for the first term on the right-hand side of equation (10). This is a physically implausible solution indicating that the numerical method will be unstable. Therefore, $\mathscr{C} = 1$ is an upper limit and a reduction in $\mathscr{C}$ to promote stability would result in a scheme that is somewhat dissipative.

3. COMPUTATIONAL METHOD

In this study, the non-linear balance equations of mass, momentum and energy are approximated using the explicit finite-difference technique of Chapman and co-workers which has been described elsewhere [5, 8]. A principal component of this computational method is the discretization of the continuity equation using the approach described by Crowley [17]. When applied to equation (1), this approach is second order accurate in both time and space. If the convection velocity (c_0 in equation (1)) is not constant, however, the accuracy of the numerical scheme is reduced. Moreover, additional dissipation is introduced by an explicit artificial viscosity [8], which is commonly needed for stability in higher order schemes. Therefore, overall second order accuracy is not expected for the system of compressible flow equations.

3.1. COMPUTATIONAL SYSTEM AND CONDITIONS

The computational approach is applied to the system depicted in Figure 1. This system is representative of an impedance tube or transmission loss bench. Acoustic disturbances are introduced at the left-hand side of the system, and the right-hand side is terminated anechoically. Two geometries are considered. A straight duct of constant cross-sectional area is studied first in order to focus on the dissipation and dispersion characteristics of the numerical method. The second geometry is a simple expansion chamber with conical area transitions which has been included to address the effects of dissipation and dispersion for a simple, yet practical silencing element.

Simulations were performed for single frequency harmonic disturbances of small amplitude (approximately 100 dB *re* 20 μPa). In order to match the conditions for inviscid linear acoustic theory, viscous shear stress and heat transfer at the duct walls were set to zero. Additional parameters for the simulations are included in Table 1. The gas properties and ambient values are consistent with air at atmospheric conditions ($c_0 = 346$ m/s), and are representative for flows in an automotive intake system.

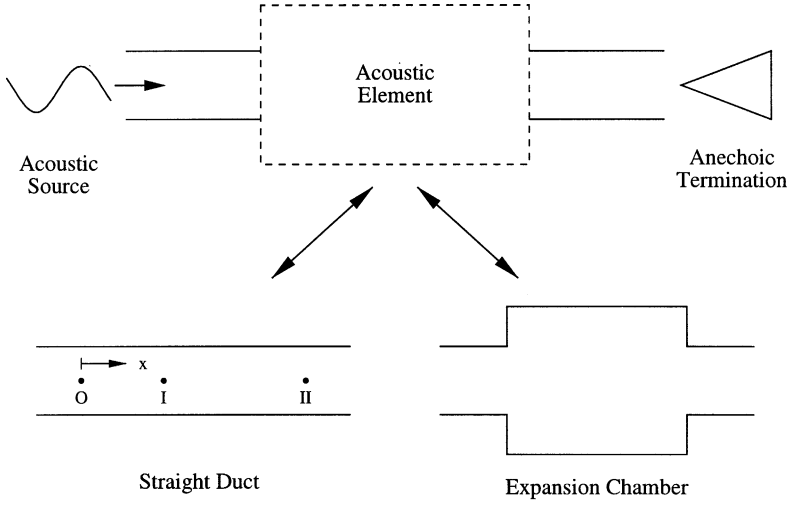

Figure 1. Geometry for computational simulations.

TABLE 1

Values for simulation variables in the computations

Variable	Description	Value
f	Frequency	25–3000 Hz
Δx	Nodal spacing	0·1–1·0 cm
$\mathscr{C}$	Courant number	0·4, 0·6, 0·8
P_0	Mean pressure	102·7 kPa
T_0	Mean temperature	298 K
R	Gas constant (Air)	287 kJ/kg K
γ	Ratio of specific heats	1·40
C_{ADF}	Artificial dissipation factor	0·5

3.2. OUTPUT DATA REDUCTION

For one-dimensional linear wave propagation in a duct of constant cross-section, the exact solution for the acoustic pressure can be described as

$$p(t) = A(f)e^{i(\omega t - kx)} + B(f)e^{i(\omega t + kx)}, \tag{11}$$

where $A(f)$ and $B(f)$ are amplitude constants representing disturbances propagating in the positive and negative directions, respectively, and, for the ideal case with no losses, $k = k_0 = \omega/c_0$. In terms of spectral components, equation (11) becomes

$$p(f) = A(f)e^{-ikx} + B(f)e^{ikx}. \tag{12}$$

Since the results of this study will be presented in terms of frequency-domain components, the frequency designation (f) will be omitted hereafter.

In many practical situations, deviations (physical or numerical) from ideal acoustic propagation over short distances are small enough to be negligible, and it may be assumed that $k = k_0$. However, in the present analysis, we wish to determine the phase and amplitude errors caused by the numerical approach. As indicated by the results from the analysis of the linear convection equation (9), deviations from the exact solution can be included by considering a complex wavenumber as

$$k = k_0 - i\alpha - \beta, \tag{13}$$

where α is a dissipation coefficient and β is a dispersion (phase error) coefficient. Thus, for a simple wave propagating in the positive direction, equations (12) and (13) give

$$p = Ae^{-i(k_0 - i\alpha - \beta)x} = Ae^{ik_0x}e^{-\alpha x}e^{i\beta x} \tag{14}$$

and the wave is attenuated as $e^{-\alpha x}$ and incurs phase error as $e^{i\beta x}$.

In order to determine the values for the dissipation and dispersion constants for the numerical method, acoustic pressures are sampled at fixed spatial locations as the time-domain computations proceed. After the computations have completed, the sampled pressures are converted into spectral components using a fast Fourier transform algorithm. Values for α and β are then obtained from the spectral components using an extension of the classic two-microphone technique [18, 19]. Since the value of k is unknown, however, acoustic pressure spectra are needed at three locations rather than two[‡]. For locations designated by O, I, and II having axial positions $x = 0$, x_I and x_{II},

[‡] With a perfectly anechoic termination, two sampling locations are sufficient. However, small reflections from the termination boundary (typically less than 1%) necessitated a three-microphone technique.

respectively (see Figure 1), the pressure spectra can be described by

$$p_0 = p(x = 0) = A + B, \tag{15}$$

$$p_{\mathrm{I}} = p(x = x_{\mathrm{I}}) = A\mathrm{e}^{-\mathrm{i}kx_{\mathrm{I}}} + B\mathrm{e}^{\mathrm{i}kx_{\mathrm{I}}}, \tag{16}$$

and

$$p_{\mathrm{II}} = p(x = x_{\mathrm{II}}) = A\mathrm{e}^{-\mathrm{i}kx_{\mathrm{II}}} + B\mathrm{e}^{\mathrm{i}kx_{\mathrm{II}}}. \tag{17}$$

Combining equations (15)–(17) to eliminate the amplitude constants and rearranging yields

$$\frac{p_{\mathrm{I}}}{p_0}(\mathrm{e}^{-\mathrm{i}kx_{\mathrm{II}}} - \mathrm{e}^{\mathrm{i}kx_{\mathrm{II}}}) + (\mathrm{e}^{-\mathrm{i}k(x_{\mathrm{I}} - x_{\mathrm{II}})} - \mathrm{e}^{\mathrm{i}k(x_{\mathrm{I}} - x_{\mathrm{II}})}) - \frac{p_{\mathrm{II}}}{p_0}(\mathrm{e}^{-\mathrm{i}kx_{\mathrm{I}}} - \mathrm{e}^{\mathrm{i}kx_{\mathrm{I}}}) = 0. \tag{18}$$

Equation (18) is a transcendental equation that can be solved to determine the complex value of k (and therefore α and β). Once k is determined, the amplitude constants may be obtained from equations (15) and (16) as in the two-microphone technique.

4. COMPUTATIONAL RESULTS

In this section, results demonstrating the dissipation and dispersion characteristics of the finite-difference technique are presented. The computational approach is first applied to simulate a simple wave propagating in a duct of constant cross-sectional area. The post-processing technique described in the preceding section is then applied to determine the dissipation and dispersion constants α and β, respectively, and investigate their behavior for different spatial resolutions and the Courant numbers. The numerical approach is then applied to an expansion chamber geometry to address the effects of numerical errors on a simple silencing element with practical importance. Discrepancies between computations and theory for the expansion chamber are then addressed in terms of the incident/transmitted pressure ratio (both magnitude and phase) as well as the transmission loss.

4.1. STRAIGHT DUCT

Straight duct simulations were performed for nodal spacings of $\Delta x = 1,\ 0{\cdot}5,\ 0{\cdot}2$ and $0{\cdot}1$ cm. The remaining computational parameters are as given in Table 1. Computed results for the dissipation constant are included in Figure 2. The values for α have been non-dimensionalized as $\alpha\lambda$ which, for a simple positive wave, represents the exponent of the dissipative term in equation (14) for a propagation distance of one wavelength. Thus, for a simple wave,

$$\frac{|p|(x = \lambda)}{|p|(x = 0)} = \mathrm{e}^{-\alpha\lambda}. \tag{19}$$

Nodal spacing is non-dimensionalized as $\Delta x/\lambda = 1/m$, where m is the number of computational cells per wavelength. The values obtained collapse to three curves representing the three different Courant numbers used. This is consistent with the findings in equation (10) for the simple first order scheme and confirms that the dissipation does not depend on the absolute value of Δx, but rather the ratios $\Delta x/\lambda$ and $\mathscr{C}$. As expected, α depends strongly on the number of cells per wavelength. The parameters in Figure 2 closely follow a linear relationship, where

$$\alpha\lambda \sim \frac{\Delta x}{\lambda} = \frac{1}{m}, \tag{20}$$

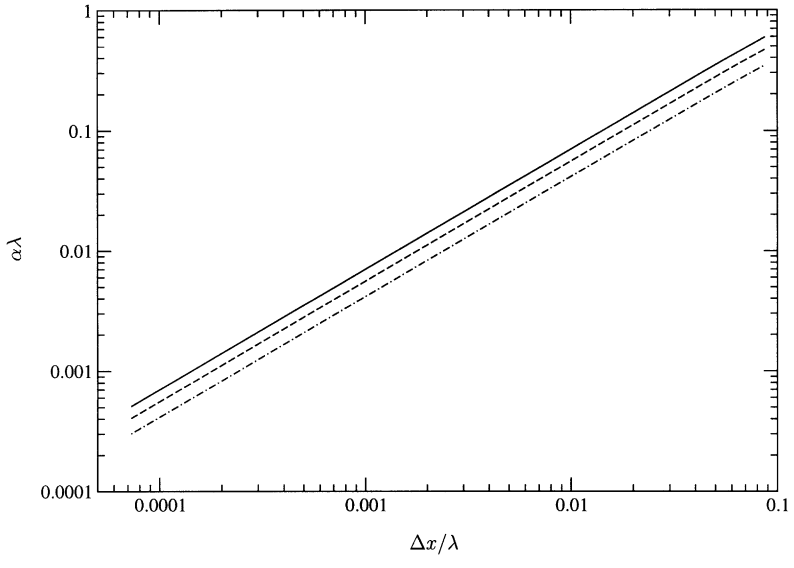

Figure 2. Non-dimensionalized dissipation constant $\alpha\lambda$ versus $\Delta x/\lambda$ for varied Courant number: ——, $\mathscr{C} = 0{\cdot}4$; – – – –, $\mathscr{C} = 0{\cdot}6$; – · – · –, $\mathscr{C} = 0{\cdot}8$.

suggesting that the overall finite-difference approach for the compressible flow equations has first order behavior (compare with the amplitude error term of equation 10). The linear relationship between α and $\Delta x/\lambda$ indicates that in terms of the sound pressure level (SPL) for a sinusoidal wave,

$$SPL = 20 \log_{10}\left(\frac{|p|/\sqrt{2}}{20\ \mu\text{Pa}}\right), \tag{21}$$

the drop in SPL for a simple wave gives

$$\Delta_{SPL} = SPL(x=0) - SPL(x) \sim \log_{10} e^{\alpha x} \sim \alpha\lambda\left(\frac{x}{\lambda}\right) \sim \left(\frac{\Delta x}{\lambda}\right)\left(\frac{x}{\lambda}\right) = \frac{1}{m}\left(\frac{x}{\lambda}\right). \tag{22}$$

Thus, for fixed $\mathscr{C}$ and frequency, the sound pressure level decreases linearly with x and the rate at which the SPL decreases is directly proportional to Δx. The results in Figure 2 also indicate a rather strong dependence of α on the Courant number. Consistent with most comparable explicit schemes, the dissipation decreases as the Courant number increases toward unity. At a particular $\Delta x/\lambda$, the value of α for $\mathscr{C} = 0{\cdot}4$ is approximately 1·7 times the value for $\mathscr{C} = 0{\cdot}8$. Therefore, in addition to using the largest Courant number possible for stability, care should be taken to ensure that $\Delta x/c$ is nearly the same for all points in the system.

Values obtained for the dispersion coefficient in the straight duct simulations are included in Figure 3. Similar to Figure 2, β is non-dimensionalized as $\beta\lambda$, and Δx is non-dimensionalized as $\Delta x/\lambda$. For the simple positive wave, $\beta\lambda$ represents the error in phase angle for a propagation distance of one wavelength. Again, as expected, the values collapse to three curves corresponding to three different Courant numbers. While a strong dependence of β on $\Delta x/\lambda$ is evident, it can be seen that the phase angle errors are less sensitive to Courant number than the dissipation errors. At a fixed value of $\Delta x/\lambda$, the variation in β between $\mathscr{C} = 0{\cdot}4$ and 0·8 is less than 10%.

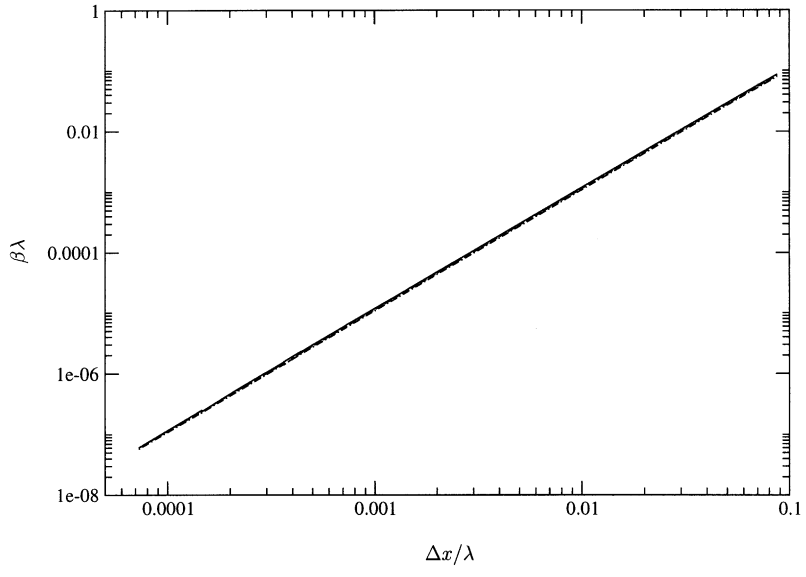

Figure 3. Non-dimensionalized dispersion coefficient ($\beta\lambda$) versus $\Delta x/\lambda$ for varied Courant number: ——, $\mathscr{C} = 0{\cdot}4$; – – – –, $\mathscr{C} = 0{\cdot}6$; – · – · –, $\mathscr{C} = 0{\cdot}8$.

For a fixed value of $\mathscr{C}$, the functional dependence between the parameters in Figure 2 is closely represented by

$$\beta\lambda \sim \left(\frac{\Delta x}{\lambda}\right)^2 = \frac{1}{m^2}, \tag{23}$$

which is consistent with the behavior of the dispersion errors found in the analysis of the first order scheme equation (10). Provided that the proportionality constant in equation (23) is not much greater than that for equation (20), dispersion errors can be expected to be of less importance than dissipation errors since $\Delta x/\lambda \ll 1$. This is confirmed by the magnitudes of $\alpha\lambda$ and $\beta\lambda$ in Figures 2 and 3. For example, with $m = 100$ computational cells per wavelength ($\Delta x/\lambda = 1/m = 0{\cdot}01$), representative values for $\alpha\lambda$ and $\beta\lambda$ are 0·05 and 0·001 respectively. Therefore, after a travel distance of 10 wavelengths, the amplitude of a simple wave will be reduced by approximately 40%, while the phase error will be approximately 0·01 rad (0·6°).

4.2. EXPANSION CHAMBER

The expansion chamber geometry modelled in this study is depicted in Figure 4. To avoid the use of boundary conditions at the ends of the expansion chamber (the area expansion and contraction), short conical transitions are used rather than area discontinuities. The three-microphone technique described earlier is applied in both the inlet and exit ducts to separate the positive and negative acoustic wave components. Results from the simulations are presented in terms of the modulus and argument of the ratio between the transmitted and incident waves (A_3/A_1) at the locations depicted in Figure 4. In addition, the transmission loss, defined as

$$TL = 20 \log_{10} \left|\frac{A_1}{A_3}\right| \tag{24}$$

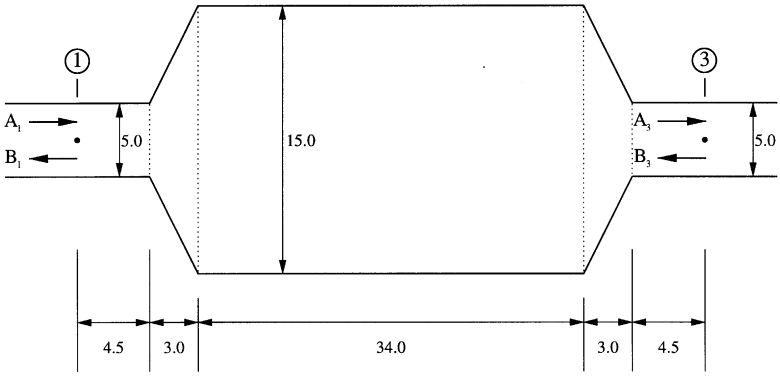

Figure 4. Expansion chamber geometry used in the simulations (dimensions in cm).

is computed and compared for the different simulations. Nodal spacings used in the expansion chamber simulations were $\Delta x = 1$ and $\frac{1}{9}$ cm. The other parameters for the expansion chamber computations are as given in Table 1.

Figures 5 and 6 include the modulus of A_3/A_1 for $\Delta x = 1$ and $\frac{1}{9}$ cm respectively. In each figure, the results for the varying Courant numbers are compared to inviscid plane wave theory. As expected, the agreement between the computations and theory is good at low frequencies, and worsens as the frequency increases ($\Delta x/\lambda$ increases). The amount of dissipation for $\Delta x = 1$ cm at higher frequencies is dramatic, particularly considering the relatively short length of the expansion chamber. A comparison of Figures 5 and 6 clearly demonstrates the reduction in dissipation when nodal spacing decreases. At higher frequencies, the effect of dissipation is most evident near the peaks in $|A_3/A_1|$, corresponding to attenuation minima for the expansion chamber. Away from these peaks, the results are less sensitive to the numerical dissipation. For all simulations, increasing the Courant number reduces dissipation, although changes in the Courant number are somewhat less significant than nodal spacing effects.

Figures 7 and 8 compare the theoretical and computed phase angle of A_3/A_1 for $\Delta x = 1$ and $\frac{1}{9}$ cm, respectively. Consistent with the straight pipe results depicted in Figure 3, phase angle discrepancies increase as $\Delta x/\lambda$ increases due to either increased frequency or nodal spacing. The small effect of the Courant number on the phase errors for the expansion chamber is also consistent with the straight pipe simulations. With consideration of the dissipation effects depicted in Figures 5 and 6, the phase errors for both nodal spacings can be seen to be comparatively insignificant for the entire frequency range considered. This confirms the findings from Figures 2 and 3 that phase errors are less likely to be of concern than dissipation.

Comparisons between the computed and theoretical transmission loss for the expansion chamber geometry are included in Figures 9 and 10. For the $\Delta x = 1$ cm simulations (Figure 9), the discrepancies between theory and computations are evident at frequencies between 500 and 1000 Hz. At higher frequencies, the dome-like behavior of the expansion chamber is lost entirely, and deviations between computations and theory are, depending somewhat on the Courant number, roughly 15–25 dB. When the nodal spacing is reduced to $\Delta x = \frac{1}{9}$ cm (Figure 10), the effects of dissipation on the transmission loss are reduced considerably. Note, for example, that the maximum deviation in transmission loss at attenuation maxima locations is approximately 1·5 dB. Dissipation effects are still evident at the higher frequency passband locations, but are, nevertheless, much improved from the $\Delta x = 1$ cm case.

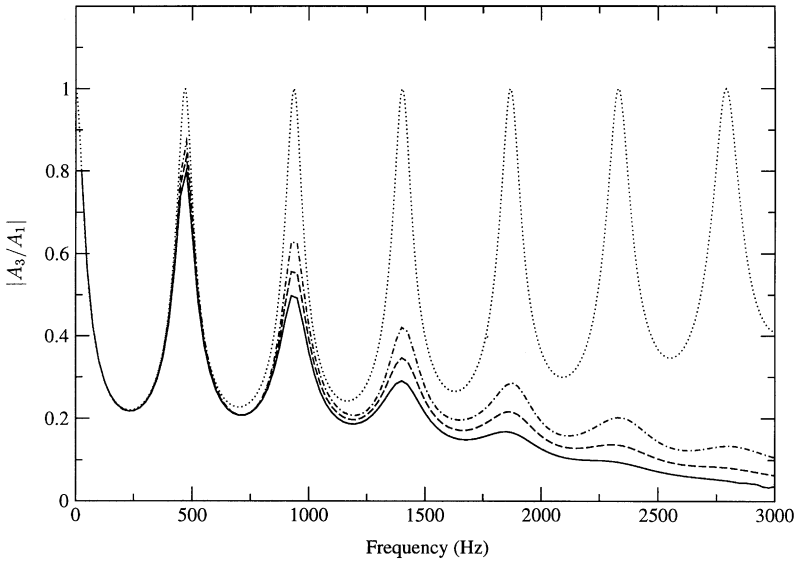

Figure 5. Modulus of transmitted/incident pressure ratio versus frequency for $\Delta x = 1$ cm and varied Courant number: ——, $\mathscr{C} = 0{\cdot}4$; – – – –, $\mathscr{C} = 0{\cdot}6$; – · – · –, $\mathscr{C} = 0{\cdot}8$; - - - - -, theory.

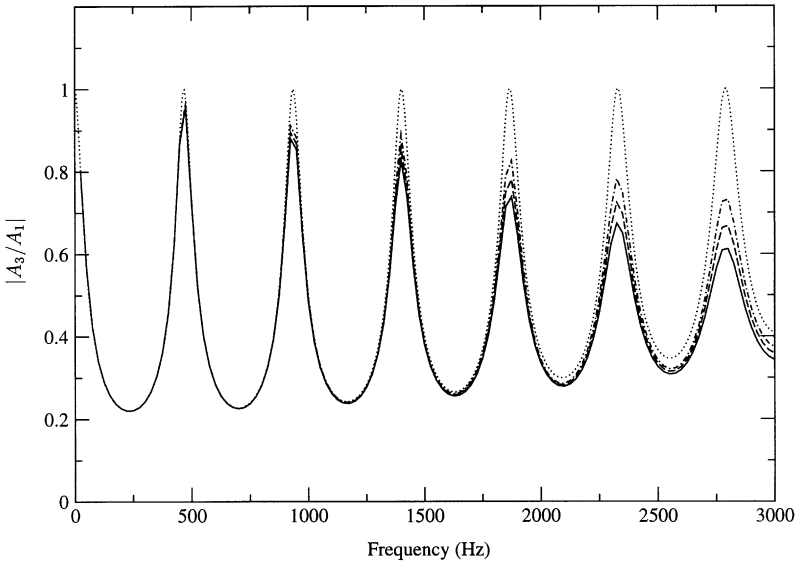

Figure 6. Modulus of transmitted/incident pressure ratio versus frequency for $\Delta x = \frac{1}{9}$ cm and varied Courant number: ——, $\mathscr{C} = 0{\cdot}4$; – – – –, $\mathscr{C} = 0{\cdot}6$; – · – · –, $\mathscr{C} = 0{\cdot}8$; - - - - -, theory.

5. CONCLUDING REMARKS

The acoustic performance of an explicit finite-difference approach for the wave dynamics in internal combustion engines has been investigated. Computational simulations of a simple wave propagating in a straight pipe and simple expansion chamber geometry demonstrated the dependence of numerical errors on both the nodal

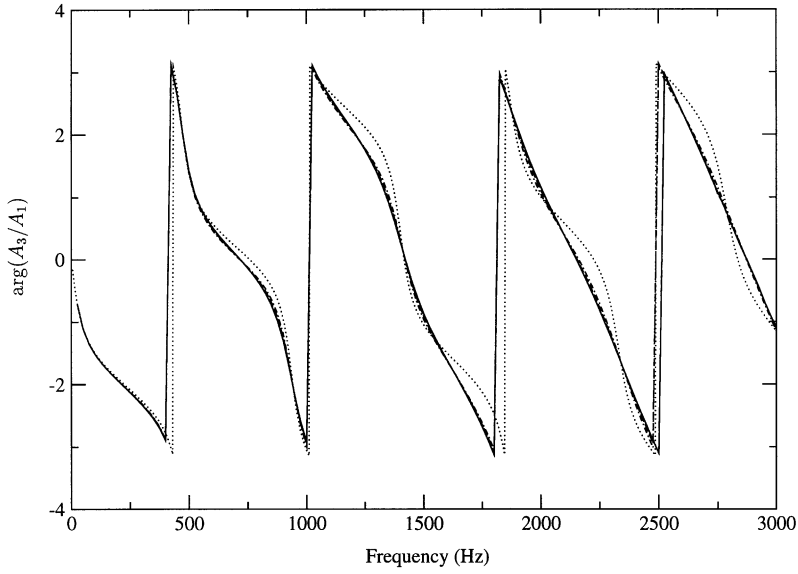

Figure 7. Argument of transmitted/incident pressure ratio versus frequency for $\Delta x = 1$ cm and varied Courant number: ——, $\mathscr{C} = 0{\cdot}4$; – – – –, $\mathscr{C} = 0{\cdot}6$; – · – · –, $\mathscr{C} = 0{\cdot}8$; - - - - -, theory.

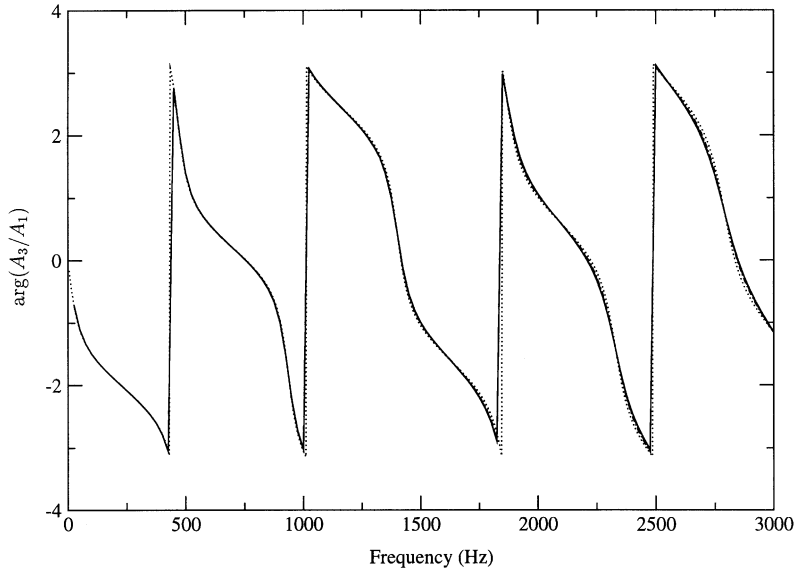

Figure 8. Argument of transmitted/incident pressure ratio versus frequency for $\Delta x = \frac{1}{9}$ cm and varied Courant number: ——, $\mathscr{C} = 0{\cdot}4$; – – – –, $\mathscr{C} = 0{\cdot}6$; – · – · –, $\mathscr{C} = 0{\cdot}8$; - - - - -, theory.

resolution ($\Delta x/\lambda$) and Courant number $\mathscr{C} = c\Delta t/\Delta x$. Dissipation was found to be highly dependent on nodal resolution with Courant number effects being less dramatic, but still very important. Phase angle errors were found to depend primarily on nodal resolution, with Courant number being relatively insignificant. For a given value of $\Delta x/\lambda$ and $\mathscr{C}$, it was demonstrated that phase angle errors are insignificant in comparison to errors caused by dissipation. Errors caused by the dissipation effects can be expected to be

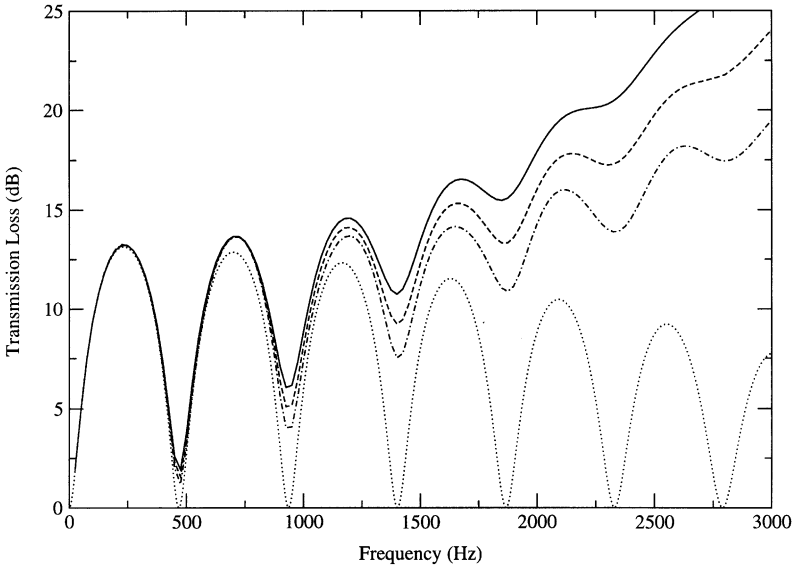

Figure 9. Transmission loss versus frequency for $\Delta x = 1$ cm and varied Courant number: ——, $\mathscr{C} = 0{\cdot}4$; – – – –, $\mathscr{C} = 0{\cdot}6$; – · – · –, $\mathscr{C} = 0{\cdot}8$; - - - - -, theory.

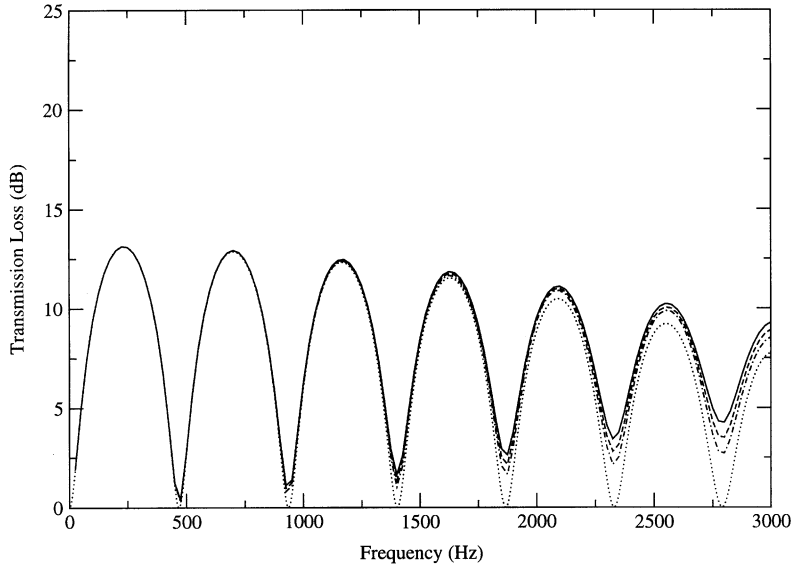

Figure 10. Transmission loss versus frequency for $\Delta x = \frac{1}{9}$ cm and varied Courant number: ——, $\mathscr{C} = 0{\cdot}4$; – – – –, $\mathscr{C} = 0{\cdot}6$; – · – · –, $\mathscr{C} = 0{\cdot}8$; - - - - -, theory.

most significant near passband locations where the actual attenuation of a reactive silencer is smallest.

For a fixed Courant number, the sound pressure level of a simple wave propagating in the positive direction was found to decrease linearly with $\Delta x/\lambda$ due to dissipation. As a

guideline for modelling an intake or exhaust system, a maximum allowable reduction in sound pressure level Δ_{SPL} for a straight duct of equivalent length can be specified. Then, using equation (22),

$$\Delta_{SPL} \sim \frac{\Delta x}{\lambda}\left(\frac{x}{\lambda}\right) = \frac{\Delta x}{c_0^2} f_{max}^2 L, \tag{25}$$

where f_{max} is the maximum frequency of interest and L is the total length of the system. For a fixed value of Δ_{SPL}, equation (25) can be viewed as

$$\Delta x \sim \frac{c_0^2}{f_{max}^2 L}. \tag{26}$$

Thus, for the same allowable Δ_{SPL} due to dissipation, (1) doubling the system length requires that Δx be reduced by a factor of two and (2) doubling the maximum frequency of interest requires that Δx be reduced by a factor of four.

The characteristics observed for this numerical scheme suggest that numerical dissipation may be an important reason that acoustic predictions from automotive simulation codes are inaccurate at higher frequencies. Effects of dissipation for the expansion chamber with $\Delta x = 1{\cdot}0$ cm (a representative nodal spacing for intake systems in practice) were dramatic, particularly considering the short length of the silencer. These results indicate that nodal spacing needs to be reduced in order to avoid high-frequency dissipation, which will result in longer computational times. Also, in order for the Courant number to be as close to unity as possible, $\Delta x/c$ should be nearly the same throughout the system. This may prove difficult in the exhaust system, since the speed of sound will vary with location and operating conditions. Finally, while the results presented in the study were obtained from a single computational technique, the general behavior is expected to be representative of a number of approaches that are currently in use for modelling the unsteady flows in automotive intake and exhaust systems.

REFERENCES

1. R. S. Benson, R. D. Garg and D. Woollatt 1964 *International Journal of Mechanical Sciences* **6**, 117–144. A numerical solution of unsteady flow problems.
2. G. A. Sod 1980 *SAE* 800288. Automotive engine modelling with a hybrid random choice method.
3. J. D. Ledger 1975 *Journal of Mechanical Engineering Science* **17**, 125–132. A finite-difference approach for solving the gas dynamics in an engine exhaust.
4. P. A. Lakshminarayanan, P. A. Janakiraman, M. K. Gajendra Babu and B. S. Murthy 1979 *SAE* 790359. Prediction of gas exchange processes in a single cylinder internal combustion engine.
5. M. Chapman, J. M. Novak and R. A. Stein 1982 Numerical modelling of inlet and exhaust flows in multi-cylinder internal combustion engines. In *Flows in Internal Combustion Engines* (Teoman Uzkan, editor). Austin, TX: ASME WAM.
6. G. Rudinger 1957 *Journal of Sound and Vibration* **3**, 48–66. The reflection of pressure waves of finite amplitude from an open end of a duct.
7. F. Payri, J. M. Desantes and A. J. Torregrosa 1995 *Journal of Sound and Vibration* **188**, 85–110. Acoustic boundary condition for unsteady one-dimensional flow calculations.
8. A. Selamet, N. S. Dickey and J. M. Novak 1994 *Journal of the Acoustical Society of America* **96**, 3177–3185. The Herschel–Quincke tube: A theoretical, computational, and experimental investigation.
9. T. Morel, M. F. Flemming and L. a. LaPointe 1990 *SAE* 900679. Characterization of manifold dynamics in the Chrysler 2.2 S.I. engine by measurements and simulation.
10. F. Payri, A. J. Torregrosa and M. D. Chust 1996 *Journal of Sound and Vibration* **195**, 757–773. Application of MacCormack schemes to I.C. engine exhaust noise prediction.

11. J. F. T. Maclaren, A. B. Tramschek, A. Sanjines and O. F. Pastrana 1975 *Journal of Mechanical Engineering Science* **17**, 271–279. A comparison of numerical solutions of the unsteady flow equations applied to reciprocating compressor systems.
12. D. E. Winterbone, R. J. Pearson and Z. Yong 1991 *Proceedings of the Institution of Mechancial Engineers Computers in Technology Conference, Cambridge*, September. Numerical simulation of intake and exhaust flows in a high-speed multi-cylinder petrol engine using the Lax-Wendroff method.
13. S. Meisner and S. C. Sorenson 1986 *SAE* 860242. Computer simulation of intake and exhaust manifold flow and heat transfer.
14. D. A. Anderson, J. C. Tannehill and R. H. Pletcher 1984 *Computational Fluid Mechanics and Heat Transfer*. Washington, DC: Hemisphere.
15. P. J. Roache 1985 *Computational Fluid Mechanics*. Albuquerque, NE: Hermosa Publishers.
16. H. Lomax, T. H. Pulliam and D. W. Zingg 2001 *Fundamentals of Computational Fluid Dynamics*. Berlin: Springer-Verlag.
17. W. P. Crowley 1967 *Journal of Computational Physics* **1**, 471–484. Second-order numerical advection.
18. A. F. Seybert and D. F. Ross 1977 *Journal of the Acoustical Society of America* **61**, 1362–1370. Experimental determination of acoustic properties using a two-microphone random-excitation technique.
19. J. Y. Chung and D. A. Blaser 1980 *Journal of the Acoustical Society of America* **68**, 907–921. Transfer function method of measuring in-duct acoustic properties. i: theory, ii: experiment.

APPENDIX A: FINITE DIFFERENCE FORM OF EQUATION (1)

Consider a continuous function p that depends on the independent variables x and t as

$$p = p(x, t). \tag{A.1}$$

A Taylor series expansion of p for a time interval Δt gives

$$p(x, t + \Delta t) = p + \frac{\partial p}{\partial t}\Delta t + \frac{\partial^2 p}{\partial t^2}\frac{(\Delta t)^2}{2!} + \frac{\partial^3 p}{\partial t^3}\frac{(\Delta t)^3}{3!} + \cdots . \tag{A.2}$$

Equation (A.2) can be rearranged as

$$\frac{\partial p}{\partial t} = \frac{p(x, t + \Delta t) - p}{\Delta t} - \frac{\partial^2 p}{\partial t^2}\frac{(\Delta t)}{2!} - \frac{\partial^3 p}{\partial t^3}\frac{(\Delta t)^2}{3!} - \cdots . \tag{A.3}$$

Neglecting all terms of order Δt and higher, gives

$$\frac{\partial p}{\partial t} = \frac{p(x, t + \Delta t) - p}{\Delta t} + O(\Delta t), \tag{A.4}$$

where the notation $O(\Delta t)^n$ is used to indicate an nth order accurate expression (the leading term that has been truncated is proportional to $(\Delta t)^n$). Using variables j and n for spatial and temporal indices, respectively, gives a first order accurate finite-difference representation of $\partial p/\partial t$ as

$$\frac{\partial p}{\partial t} = \frac{p_j^{n+1} - p_j^n}{\Delta t} + O(\Delta t). \tag{A.5}$$

A Taylor series expansion of p with respect to x for the interval $-\Delta x$ gives

$$p(x - \Delta x, t) = p - \frac{\partial p}{\partial x}\Delta x + \frac{\partial^2 p}{\partial x^2}\frac{(\Delta x)^2}{2!} - \frac{\partial^3 p}{\partial x^3}\frac{(\Delta x)^3}{3!} + \cdots . \tag{A.6}$$

Equation (A.6) can be rearranged to give a first order accurate representation for $\partial p/\partial x$ as

$$\frac{\partial p}{\partial x} = \frac{p_j^n - p_{j-1}^n}{\Delta x} + O(\Delta x). \tag{A.7}$$

Inserting equations (A.5) and (A.7) into equation (1) gives a finite difference representation of the linear convection equation as

$$\frac{p_j^{n+1} - p_j^n}{\Delta t} + c_0 \frac{p_j^n - p_{j-1}^n}{\Delta x} + O(\Delta t, \Delta x) = 0, \tag{A.8}$$

which has first order accuracy in both Δt and Δx.